Performance Analysis of Collaborative Positioning Method in Automated Car Driving

Shuo Li[a], Nikolay Mikhaylov[a], Florian Schiegg[a] and Yichen Liu[a]

[a] *Robert Bosch GmbH, Robert-Bosch-Straße 200, Hildesheim, Germany*

Abstract

Automated car driving is a complex project involving many technologies, and it is essential to obtain vehicles' accurate position information by using Global Navigation Satellite System (GNSS) technology. However, in many scenarios, such as urban canyon, it is difficult for vehicles to acquire accurate positioning results through stand-alone Single Point Positioning (SPP) due to obstruction and lacking visible satellites. With the rapid development of GNSS technology and Vehicle to Everything (V2X) communication, the GNSS Collaborative Positioning (CoPos) is becoming possible. CoPos requires vehicles to share GNSS raw measurements with their neighbors through V2X communication and to measure the local ranges between vehicles. In this paper, basic GNSS pseudorange and local range observation equations, Extended Kalman Filter (EKF) positioning algorithm and a Non-Line-of-Sight (NLOS) detection algorithm for CoPos are presented. A simulation framework based on vehicle dynamics simulator CarMaker and GNSS simulator Spirent is designed. Performance analysis of CoPos is offered in terms of a defined Collaborative Dilution of Precision (CDOP) value and positioning results compared with SPP. The results of the NLOS detection algorithm are given too. It is shown that the developed CoPos and NLOS-detection algorithms provide better positioning results than standard stand-alone SPP.

Keywords

GNSS, V2X, Collaborative Positioning, Extended Kalman Filter, Multipath Detection, Simulation Framework, CarMaker, Spirent, Performance Analysis

1. Introduction

Global Navigation Satellite System (GNSS) refers to a constellation of satellites that provides autonomous geo-spatial positioning with global coverage and it has been widely used in various fields such as transportation, navigation, surveying and rescue, etc. An automated driving system is a complex combination of various technologies and a fully autonomous vehicle needs an accurate, reliable, redundant and continuous positioning solution from GNSS. However, facing occlusions and multipath effects in urban canyons, tunnels forests and other challenging environments, the positioning performance would be affected severely and up to now, there are no good solutions in these scenarios for stand-alone Single Point Positioning (SPP) [1]. To overcome it, with the development of communication and ranging technology, many positioning methods have been proposed with the assumption that the positions of some base stations are known. For example, base stations can transmit corrections to a moving vehicle, the vehicle can fix the positioning result with higher accuracy by utilizing these corrections. However, it is difficult to set a large network of base stations, and as a result, the coverage of the base stations is limited, compared with GNSS [2].

ICL-GNSS 2020 WiP Proceedings, June 02–04, 2020, Tampere, Finland
EMAIL: shuo.li.chn@gmail.com (A. 1); Nikolay.Mikhaylov@de.bosch.com (A. 2); Florian.Schiegg@de.bosch.com (A. 3); yichen.liu@tum.de (A. 4)
ORCID: 0000-0002-6826-3291 (A. 1); 0000-0001-9184-3465 (A. 2); 0000-0002-6889-4878 (A. 3); 0000-0003-0253-9520 (A. 4)

Driven by the development of Vehicle to Everything (V2X) communication technology, Collaborative Positioning (CoPos) provides an alternative solution to solve this problem. CoPos refers to a group of users sharing their raw GNSS measurements and measuring the local ranges with their neighboring users to accomplish positioning. CoPos can improve the positioning performance such as availability, continuity, and accuracy [3, 4]. GNSS has global coverage, therefore it can resolve the coverage issue of wireless sensor networks. Apart from GNSS measurement, a precise local range measurement is essential to achieve a better performance of CoPos. For almost a decade, multi-sensors have been available in vehicles, for example, a prototype of a fully autonomous vehicle is proposed in [5] using 3D laser scanners to obtain an accurate position of the surrounding environment. Different sensors have their advantages and disadvantages and an intelligent strategy is to do the data fusion, combining the measurements from different sensors and from V2X messages, such as the collective perception message currently being standardized by the European Telecommunications Standards Institute [6], in order to obtain a more precise local range measurement.

Several multipath mitigation methods are introduced in [7], they can be classified as antenna-based, receiver-based and post-receiver. The antenna-based method can attenuate reflected signals, but it has a little effect on positioning errors caused by Non-Line-of-Sight (NLOS) signals, moreover, advanced antennas are bulky and expensive. Receiver-based techniques can reduce the positioning errors significantly by sharpening the peak of the code correlation function, but it does not affect NLOS signal reception. Post-receiver technology compares measurements in different frequencies or code and phase measurements to detect NLOS signals.

In this work, a combination of GNSS and V2X technology to obtain vehicles' positioning solution is introduced. A CoPos algorithm in [8] is extended by Extended Kalman Filter (EKF) and a defined Collaborative Dilution of Precision (CDOP) based on [9] are presented. In section 3, a multipath detection algorithm proposed in [10] is modified for EKF-based CoPos. The used simulation framework based on the simulator TEPLITS [11,12] is described in section 4, section 5 gives the performance analysis of CoPos compared with SPP. Finally, the conclusions are given in the section 6.

2. Collaborative Positioning

Figure 1 shows a typical collaborative positioning of a multi-user application scenario. In an urban environment, satellite visibility could be bad because of building blockage, and the multipath effect is strong. As shown in Figure 1, the vehicle located in the middle tracks less than four satellites because GNSS signals are blocked by the tall building. As a result, the basic requirement to perform SPP is not fulfilled. However, the considered vehicle communicates with the other two vehicles through V2X. Each of the other two vehicles tracks four satellites and transmits GNSS raw measurements as well as pre-processed data via V2X messages. The considered vehicle in the middle receives messages from other vehicles and measures local range to the other two vehicles.

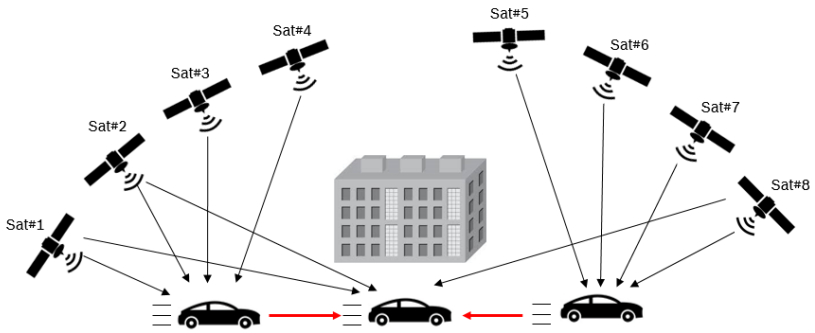

Figure 1: A typical multi-user application scenario

The basic pseudorange observation equation of user u and satellite k can be expressed as

$$\rho_u^k = d_u^k + c\delta t_u - c\delta t^k + \varepsilon_u^k, \quad (1)$$

where ρ_u^k is pseudorange measurement, d_u^k is true range between user u and satellite k, c is speed of light, δt_u and δt^k are receiver clock bias and satellite clock bias respectively, ε_u^k includes atmospheric delay, multipath, receiver noise and satellite orbital errors.

The local range observation equation is given by

$$r_{i,j} = d_{i,j} + \eta_{i,j}, \tag{2}$$

where $r_{i,j}$ is local range measurement, $d_{i,j}$ is the true range from user i to user j and $\eta_{i,j}$ is local range measurement noise. In general, $\eta_{i,j}$ depends on the ranging technology and the changing user environment. Typically, a meter level accuracy of local range measurements can be achieved and for some high accuracy ranging technologies or through data fusion, a centimeter-level accuracy can be obtained.

Based on the aforementioned pseudorange and local range observation equations, a CoPos algorithm using EKF is implemented. The EKF produces firstly estimates of the current state variables, along with their uncertainties, once the next measurement is observed, these estimates are updated using a weighted average. The algorithm is divided into four steps.

- Set initial state vector and covariance matrix

The initial state vector $\hat{\boldsymbol{x}}_{0,1}$ of user 1 can be set as

$$\hat{\boldsymbol{x}}_{0,1} = \left[x_1, \dot{x}_1, y_1, \dot{y}_1, z_1, \dot{z}_1, c\delta t_1, c\dot{\delta} t_1\right], \tag{3}$$

where x_1, y_1, z_1 are the user's position, $\dot{x}_1$, $\dot{y}_1$, $\dot{z}_1$ are the user's velocity and $c\delta t_1, c\dot{\delta} t_1$ are clock bias and clock bias drift of user 1. The over dots denote the time derivative. Consider the number of users in a group is n, the initial state vector $\hat{\boldsymbol{x}}_0$ is the combination of the state vectors of all users and it is a $8n \times 1$ matrix

$$\hat{\boldsymbol{x}}_0 = \left[\hat{\boldsymbol{x}}_{0,1}, \hat{\boldsymbol{x}}_{0,2}, \ldots, \hat{\boldsymbol{x}}_{0,n}\right]^T. \tag{4}$$

The initial error covariance matrix $\boldsymbol{P}_0$ indicates the degree of trust in the current state, and a relatively small value is generally set in order to obtain a fast convergence speed. The initial $\boldsymbol{P}_0$ matrix can be set as an $8n \times 8n$ identity matrix

$$\boldsymbol{P}_0 = \begin{bmatrix} 1 & \cdots & 0 \\ \vdots & \ddots & \vdots \\ 0 & \cdots & 1 \end{bmatrix}. \tag{5}$$

- Prediction

The prediction of state vector and covariance matrix can be expressed as

$$\begin{aligned} \hat{\boldsymbol{x}}_t^- &= \boldsymbol{A}\hat{\boldsymbol{x}}_{t-1} \\ \boldsymbol{P}_t^- &= \boldsymbol{A}\boldsymbol{P}_{t-1}\boldsymbol{A}^T + \boldsymbol{Q}, \end{aligned} \tag{6}$$

where $\hat{\boldsymbol{x}}_t^-$, $\boldsymbol{P}_t^-$ are the predicted state vector and error covariance of current epoch t, $\hat{\boldsymbol{x}}_{t-1}, \boldsymbol{P}_{t-1}$ are the state vector and error covariance of previous epoch $t-1$, $\boldsymbol{A}$ is a $8n \times 8n$ state transition matrix, it is a block diagonal matrix of the form

$$\boldsymbol{A} = \begin{bmatrix} \boldsymbol{A}_{xyzb} & \cdots & \boldsymbol{0} \\ \vdots & \ddots & \vdots \\ \boldsymbol{0} & \cdots & \boldsymbol{A}_{xyzb} \end{bmatrix}, \tag{7}$$

where $\boldsymbol{A}_{xyzb}$ is state transition matrix of one user. Based on a simple constant velocity model and assuming there is no coupling between x, y, z and $c\delta t$, $\boldsymbol{A}_{xyzb}$ is formed by

$$\boldsymbol{A}_{xyzb} = \begin{bmatrix} \boldsymbol{A}_{xyz} & \boldsymbol{0} & \boldsymbol{0} & \boldsymbol{0} \\ \boldsymbol{0} & \boldsymbol{A}_{xyz} & \boldsymbol{0} & \boldsymbol{0} \\ \boldsymbol{0} & \boldsymbol{0} & \boldsymbol{A}_{xyz} & \boldsymbol{0} \\ \boldsymbol{0} & \boldsymbol{0} & \boldsymbol{0} & \boldsymbol{A}_b \end{bmatrix}, \tag{8}$$

where

$$\boldsymbol{A}_{xyz} = \boldsymbol{A}_b = \begin{bmatrix} 1 & \Delta t \\ 0 & 1 \end{bmatrix}. \tag{9}$$

$\boldsymbol{Q}$ is covariance matrix of the process noise, the smaller value in $\boldsymbol{Q}$ matrix indicates the higher degree of trust in the predicted state. On the contrary, the larger value in $\boldsymbol{Q}$ represents the higher confidence in the measurements. The process covariance matrix $\boldsymbol{Q}_{xyzb}$ of one user is a block diagonal matrix with three identical submatrices for the position-velocity pairs and one submatrix for the clock-clock drift pair. The forming of $\boldsymbol{Q}_{xyzb}$ matrix assumes that the states are uncorrelated with each other outside of the pairs and statistically coupled only in pairs

$$\boldsymbol{Q}_{xyzb} = \begin{bmatrix} \boldsymbol{Q}_{xyz} & \boldsymbol{0} & \boldsymbol{0} & \boldsymbol{0} \\ \boldsymbol{0} & \boldsymbol{Q}_{xyz} & \boldsymbol{0} & \boldsymbol{0} \\ \boldsymbol{0} & \boldsymbol{0} & \boldsymbol{Q}_{xyz} & \boldsymbol{0} \\ \boldsymbol{0} & \boldsymbol{0} & \boldsymbol{0} & \boldsymbol{Q}_b \end{bmatrix}. \tag{10}$$

We follow work [13] to set $\boldsymbol{Q}_{xyz}$ and $\boldsymbol{Q}_b$. A white noise spectral density which represents random walk velocity error can be defined as σ_{xyz}^2, and each position-velocity pair has two variance terms and one covariance term, which describes a submatrix

$$\boldsymbol{Q}_{xyz} = \sigma_{xyz}^2 \begin{bmatrix} \frac{\Delta t^3}{3} & \frac{\Delta t^2}{2} \\ \frac{\Delta t^2}{2} & \Delta t \end{bmatrix}. \tag{11}$$

A clock-clock drift pair has two variance terms and one covariance term as well. Two components of clock phase error S_f, the white noise spectral density leading to random walk velocity error and S_g, the white noise spectral density leading to a random walk clock frequency error plus white noise clock drift form another submatrix together

$$\boldsymbol{Q}_b = \begin{bmatrix} S_f \Delta t + \frac{S_g \Delta t^3}{3} & \frac{S_g \Delta t^2}{2} \\ \frac{S_g \Delta t^2}{2} & S_g \Delta t \end{bmatrix}. \tag{12}$$

The process noise covariance matrix $\boldsymbol{Q}$ is a $8n \times 8n$ matrix and it is the combination of $\boldsymbol{Q}_{xyzb}$ of all users

$$\boldsymbol{Q} = \begin{bmatrix} \boldsymbol{Q}_{xyzb} & \cdots & \boldsymbol{0} \\ \vdots & \ddots & \vdots \\ \boldsymbol{0} & \cdots & \boldsymbol{Q}_{xyzb} \end{bmatrix}. \tag{13}$$

- Compute Kalman gain

After predicting, the next step is to compute the Kalman gain $\boldsymbol{K}_t$

$$\boldsymbol{K}_t = \boldsymbol{P}_t^- \boldsymbol{G}^T (\boldsymbol{G}\boldsymbol{P}_t^- \boldsymbol{G}^T + \boldsymbol{R})^{-1}, \tag{14}$$

where $\boldsymbol{G}$ is geometry matrix of the observation model, $\boldsymbol{R}$ is measurement error covariance matrix. $\boldsymbol{G}$ matrix can be expanded as

$$\boldsymbol{G} = \begin{bmatrix} \boldsymbol{G}_\rho \\ \boldsymbol{G}_r \end{bmatrix}, \tag{15}$$

the construction of submatrices $\boldsymbol{G}_\rho$ and $\boldsymbol{G}_r$ are based on the observation equations (1) and (2). Since the pseudorange and local range observation equations are nonlinear in the receiver position coordinates, a Taylor series expansion is applied. The geometry matrix of pseudorange $\boldsymbol{G}_\rho$ can be built by

$$\boldsymbol{G}_{\rho} = \begin{bmatrix} \boldsymbol{G}_{\rho,1} & \cdots & \boldsymbol{0} \\ \vdots & \ddots & \vdots \\ \boldsymbol{0} & \cdots & \boldsymbol{G}_{\rho,n} \end{bmatrix} \quad \boldsymbol{G}_{\rho,1} = \begin{bmatrix} \boldsymbol{e}_1^1 & 1 & 0 \\ \vdots & \vdots & \vdots \\ \boldsymbol{e}_1^{k_1} & 1 & 0 \end{bmatrix}, \tag{16}$$

where $\boldsymbol{G}_{\rho,1}$ is geometry matrix of user 1, k_1 is the number of pseudorange measurements of user 1, $\boldsymbol{e}_1^1$ is given by

$$\boldsymbol{e}_1^1 = \left[\frac{x_1 - x^1}{d_1^1}, 0, \frac{y_1 - y^1}{d_1^1}, 0, \frac{z_1 - z^1}{d_1^1}, 0 \right], \tag{17}$$

where x^1, y^1, z^1 describe the position of satellite 1. The geometry matrix of local range $\boldsymbol{G}_r$ can be built by

$$\boldsymbol{G}_r = \begin{bmatrix} \boldsymbol{e}_{1,2} & -\boldsymbol{e}_{1,2} & \boldsymbol{0} & \ldots & \ldots & \boldsymbol{0} \\ \boldsymbol{e}_{1,3} & \boldsymbol{0} & -\boldsymbol{e}_{1,3} & \boldsymbol{0} & \ldots & \boldsymbol{0} \\ \vdots & \vdots & \vdots & \vdots & \vdots & \vdots \\ \boldsymbol{e}_{1,n} & \boldsymbol{0} & \boldsymbol{0} & \boldsymbol{0} & \ldots & -\boldsymbol{e}_{1,n} \end{bmatrix}, \tag{18}$$

where

$$\boldsymbol{e}_{1,2} = \left[\frac{x_1 - x_2}{d_{1,2}}, 0, \frac{y_1 - y_2}{d_{1,2}}, 0, \frac{z_1 - z_2}{d_{1,2}}, 0, 0, 0 \right]. \tag{19}$$

Assuming the number of pseudorange measurements of the user group is N, $\boldsymbol{G}$ is a $(N + n - 1) \times 8n$ matrix.

The determination of the $\boldsymbol{R}$ matrix is related to the noise of the measurements. $\boldsymbol{R}_{\rho}$ and $\boldsymbol{R}_r$ are submatrices of $\boldsymbol{R}$ matrix, representing measurement error of pseudorange and local range respectively

$$\boldsymbol{R} = \begin{bmatrix} \boldsymbol{R}_{\rho} & \boldsymbol{0} \\ \boldsymbol{0} & \boldsymbol{R}_r \end{bmatrix}. \tag{20}$$

The pseudorange measurement errors come from various sources, so it is difficult to get the probability distribution of the measurement errors. However, the standard deviation of pseudorange measurement error σ_{ρ} can be calculated using the measured carrier-to-noise-density ratio ($C/N0$). In [14], a stochastic SIGMA $-$ Δ model is proposed

$$\sigma_{\rho}^2 = \mathrm{C}_m \cdot 10^{-(C/N0)/10}, \tag{21}$$

where m indicates the L_m signal (L_1 or L_2) and the effect of the oscillator stability on the phase variances is considered negligible. C_m consists of the carrier loop noise bandwidth and a conversion term from cycle to meter which includes the L_m wavelength. Under the assumption that the pseudorange measurement errors are uncorrelated with each other, the $\boldsymbol{R}_{\rho}$ is a $N \times N$ diagonal matrix. The local range measurement error σ_r depends on sensor error models. Assuming the local range measurement errors are independent, the $\boldsymbol{R}_r$ is a $(n-1) \times (n-1)$ diagonal matrix as well

$$\boldsymbol{R}_{\rho} = \begin{bmatrix} \boldsymbol{\Sigma}_{\rho,1}^2 & \cdots & \boldsymbol{0} \\ \vdots & \ddots & \vdots \\ \boldsymbol{0} & \cdots & \boldsymbol{\Sigma}_{\rho,n}^2 \end{bmatrix} \quad \boldsymbol{R}_r = \begin{bmatrix} \sigma_{r,1,2}^2 & \cdots & 0 \\ \vdots & \ddots & \vdots \\ 0 & \cdots & \sigma_{r,1,n}^2 \end{bmatrix}, \tag{22}$$

where $\sigma_{r,1,2}^2$ is error square of local range measurement from user 1 to user 2, $\boldsymbol{\Sigma}_{\rho,1}^2$ is a block diagonal matrix of the form

$$\boldsymbol{\Sigma}_{\rho,1}^2 = \begin{bmatrix} \sigma_{\rho,1,1}^2 & \cdots & 0 \\ \vdots & \ddots & \vdots \\ 0 & \cdots & \sigma_{\rho,1,k_1}^2 \end{bmatrix}, \tag{23}$$

where $\sigma_{\rho,1,1}^2$ is pseudorange measurement error square of satellite 1 tracked by user 1.

- Update

The last step is to update the estimated state vector and error covariance

$$\hat{\boldsymbol{x}}_t = \hat{\boldsymbol{x}}_t^- + \boldsymbol{K}_t(\boldsymbol{z}_t - \boldsymbol{G}\hat{\boldsymbol{x}}_t^-)$$
$$\boldsymbol{P}_t = \boldsymbol{P}_t^- - \boldsymbol{K}_t\boldsymbol{G}\boldsymbol{P}_t^-, \tag{24}$$

where $\boldsymbol{z}_t$ is pseudorange and local range measurements. In this step, the estimated user state vector and error covariance matrix will be updated and they can be set as the initials for the next measurement epoch.

There are many factors that affect the satellite positioning accuracy and it makes the theoretical performance analysis difficult. Therefore, a Dilution of Precision (DOP) is used to simplify the analysis process. DOP is an important factor used to determine the positioning accuracy, but it only depends on the geometry of the satellites. To analyze the impact of both satellite geometry and user geometry, a CDOP is proposed in [9]. A collaborative weight coefficient matrix $\boldsymbol{H}$ can be computed by using geometry matrix defined in (15).

$$\boldsymbol{H} = (\boldsymbol{G}^T\boldsymbol{R}\boldsymbol{G})^{-1}. \tag{25}$$

Matrix $\boldsymbol{H}$ contains the contributions from the number of users in a user group, user distributions, visible satellites from each user and satellite geometries. The diagonal elements of matrix $\boldsymbol{H}$ are the variances of estimated users' position and clock bias, the off-diagonal elements indicate the degree of correlation. It can be expanded as

$$\boldsymbol{H} = \begin{bmatrix} \boldsymbol{H}_1 & \boldsymbol{H}_{1,2} & \cdots & \boldsymbol{H}_{1,n} \\ \boldsymbol{H}_{2,1} & \boldsymbol{H}_2 & \ldots & \boldsymbol{H}_{2,n} \\ \vdots & \vdots & \ddots & \vdots \\ \boldsymbol{H}_{n,1} & \boldsymbol{H}_{n,2} & \cdots & \boldsymbol{H}_n \end{bmatrix}, \tag{26}$$

where $\boldsymbol{H}_1$ is the collaborative weight coefficient matrix for the user 1. The Collaborative Geometric Dilution of Precision (CGDOP) of user 1 is defined as

$$CGDOP_1 = \sqrt{h_{1,11} + h_{1,22} + h_{1,33} + h_{1,44}}, \tag{27}$$

where $h_{1,11}$ is the first diagonal elements of $\boldsymbol{H}_1$. In order to get Collaborative East Dilution of Precision (CEDOP) and Collaborative North Dilution of Precision (CNDOP), the current earth-centered-earth-fixed coordinate should be transformed to east–north–under coordinate system by an orthogonal rotation matrix [15].

$$CEDOP_1 = \sqrt{h'_{1,11}} \qquad CNDOP_1 = \sqrt{h'_{1,22}}, \tag{28}$$

where $h'_{1,11}$ represent the first diagonal elements of $\boldsymbol{H}_1$ after transformation.

3. Multipath Detection

As mentioned in [10], NLOS and multipath-contaminated measurements produce a less consistent navigation solution than direct Line-of-Sight (LOS) measurements. Multipath detection aims to identify the set of measurements, which are affected by multipath and to either discard them or reduce their weight in (20) when calculating the position of users. Therefore, the multipath detection algorithm can be merged into the EKF after the prediction step.

A new vector $\boldsymbol{\zeta}_1^{k_1}$ combining pseudorange measurements and local range measurements of user 1 can be defined according to (1) and (2)

$$\boldsymbol{\zeta}_1^{k_1} = \begin{bmatrix} \boldsymbol{\rho}_1^{k_1} \\ \boldsymbol{r}_{1,n} \end{bmatrix}$$
$$\boldsymbol{\zeta}_1^{k_1} = \begin{bmatrix} \boldsymbol{d}_1^{k_1} \\ \boldsymbol{d}_{1,n} \end{bmatrix} + \boldsymbol{G}'\Delta\hat{\boldsymbol{x}}_t'^- + \begin{bmatrix} c\delta\boldsymbol{t}_1 \\ \boldsymbol{0} \end{bmatrix} + \begin{bmatrix} \boldsymbol{\sigma}_{\rho,1}^2 \\ \boldsymbol{\sigma}_{r,1}^2 \end{bmatrix} + \begin{bmatrix} \boldsymbol{\tau}_{k_1} \\ \boldsymbol{0} \end{bmatrix}, \tag{29}$$

where $\boldsymbol{\tau}_{k_1}$ is NLOS delay, $\Delta\hat{\boldsymbol{x}}_t'^-$ is the predicted state error without clock terms and $\boldsymbol{G}'$ is similar to (15)

$$\Delta\hat{\boldsymbol{x}}_t'^- = [\Delta\hat{x}_t'^-, 0, \Delta\hat{y}_t'^-, 0, \Delta z_t'^-, 0]^T$$
$$\boldsymbol{G}' = \left[\boldsymbol{e}_1^1, \dots, \boldsymbol{e}_1^{k_1}, \boldsymbol{e}_{1,2}', \dots, \boldsymbol{e}_{1,n}'\right]^T. \tag{30}$$

where $\boldsymbol{e}_{1,2}'$ is the first six elements of $\boldsymbol{e}_{1,2}$ in (19). Since the components constructing $\boldsymbol{\zeta}_1^{k_1}$ are independent and considering the pseudorange measurements and the local range measurements are independent as well, the distribution of the vector $\boldsymbol{\zeta}_1^{k_1}$ is expressed as

$$\boldsymbol{\zeta}_1^{k_1} \sim \mathcal{N}(\boldsymbol{D}, \boldsymbol{V}), \tag{31}$$

where

$$\boldsymbol{D} = \begin{bmatrix} \boldsymbol{d}_1^{k_1} \\ \boldsymbol{d}_{1,n} \end{bmatrix} + \begin{bmatrix} c\delta\boldsymbol{t}_1 \\ \boldsymbol{0} \end{bmatrix} + \begin{bmatrix} \boldsymbol{\tau}_{k_1} \\ \boldsymbol{0} \end{bmatrix}$$
$$\boldsymbol{V} = \boldsymbol{G}'\boldsymbol{\Lambda}\boldsymbol{G}'^T + \begin{bmatrix} \boldsymbol{\Sigma}_{\rho,1}^2 & \boldsymbol{0} \\ \boldsymbol{0} & \boldsymbol{R}_r \end{bmatrix}. \tag{32}$$

The covariance matrix $\boldsymbol{\Lambda}$ of predicted state error $\Delta\hat{\boldsymbol{x}}_t'^-$ is diagonal matrix. By comparing the $C/N0$ to the preset threshold, the vector $\boldsymbol{\zeta}_1^{k_1}$ can be divided into two groups, one contains ϕ_1 possible NLOS measurements and the other has ϕ_2 LOS measurements and local range measurements in total. The measurements in group 1 and group 2 can be approximated by a Gaussian distribution

$$\boldsymbol{\zeta}_1^{k_1} = \begin{bmatrix} \boldsymbol{\zeta}_{\phi_1} \\ \boldsymbol{\zeta}_{\phi_2} \end{bmatrix} \sim \left(\begin{bmatrix} \boldsymbol{D}_1 \\ \boldsymbol{D}_2 \end{bmatrix}, \begin{bmatrix} \boldsymbol{V}_{11} & \boldsymbol{V}_{12} \\ \boldsymbol{V}_{21} & \boldsymbol{V}_{22} \end{bmatrix} \right), \tag{33}$$

the size of $\boldsymbol{D}_1$, $\boldsymbol{D}_2$, $\boldsymbol{V}_{11}$, $\boldsymbol{V}_{12}$, $\boldsymbol{V}_{21}$ and $\boldsymbol{V}_{22}$ are $\phi_1 \times 1$, $\phi_2 \times 1$, $\phi_1 \times \phi_1$, $\phi_1 \times \phi_2$, $\phi_2 \times \phi_1$ and $\phi_2 \times \phi_2$ respectively. If there is no NLOS delay in group 1, the conditional variable $\boldsymbol{\zeta}_{\phi_1} | \boldsymbol{\zeta}_{\phi_2}$ should have a conditional Gaussian distribution [16] with mean $\boldsymbol{\mu}_{\phi_1}$ and variance $\boldsymbol{V}_{\phi_1}$

$$\boldsymbol{\mu}_{\phi_1} = \boldsymbol{D}_1 + \boldsymbol{V}_{12}\boldsymbol{V}_{22}^{-1}\left(\boldsymbol{\zeta}_{\phi_2} - \boldsymbol{D}_2\right)$$
$$\boldsymbol{V}_{\phi_1} = \boldsymbol{V}_{11} - \boldsymbol{V}_{12}\boldsymbol{V}_{22}^{-1}\boldsymbol{V}_{21}. \tag{34}$$

Therefore, a normalized detection variable Z_{ϕ_1} is defined to check if the pseudorange measurements in group 1 are corrupted by NLOS delays. Z_{ϕ_1} is the square of the Mahalanobis distance (MD)

$$Z_{\phi_1} = \left(\boldsymbol{\zeta}_{\phi_1} - \boldsymbol{\mu}_{\phi_1}\right)^T \boldsymbol{V}_{\phi_1}^{-1} \left(\left(\boldsymbol{\zeta}_{\phi_1} - \boldsymbol{\mu}_{\phi_1}\right)\right). \tag{35}$$

If the detection statistics has a noncentral χ^2 distribution with degree of freedom of ϕ_1, the pseudorange measurements in group 1 contain NLOS delay. Otherwise, there is no NLOS delay in group 1. However, Z_{ϕ_1} is only the sum of MD squares of all measurements in group 1. In order to distinguish which measurement is corrupted by NLOS delay, the presented multipath detection algorithm should be applied to each measurement individually. If one measurement has delay caused by NLOS, the corresponding variance of pseudorange measurement error in (22) should be changed to reduce the weight of this measurement in positioning.

4. Simulation Framework

To analyze the performance of CoPos, a Matlab-based simulation framework is set up according to the TEPLITS simulator, that is based on the dedicated vehicle dynamic simulator CarMaker and the GNSS simulator Spirent.

- Carmaker

CarMaker, developed by IPG Automotive, is an advanced software package for model-based design, testing, and development in the field of vehicle dynamics. It provides powerful and real-time capable

models for vehicles, roads, drivers and traffic. Using CarMaker, real-world test scenarios including the entire surrounding environment can be modeled accurately. When running the simulation, it is possible to visualize real-time quantities of vehicle model, trailer, brake system, powertrain, driving maneuver, etc. by IPG-Control. Vehicle motion parameters including position, velocity and acceleration can be recorded into user motion files, which can be used as input for Spirent simulator to generate GNSS measurements. Besides, an ideal local range measurement can be computed by using the reference coordinates in the user motion files of every two vehicles. Measurements of sensors are accessible as well. The fused sensor distance measurement can be later used as a local range measurement for CoPos.

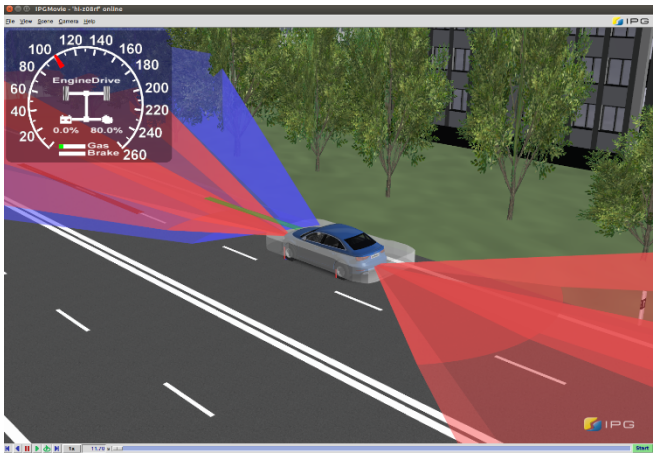

Figure 2: A Simple CarMaker scenario with a vehicle equipped with sensors

- Spirent

Spirent GNSS simulator is widely used to simulate the GNSS constellations, transmitted signals and received signals by a static or dynamic receiver. It enables receiver performance test in a controlled laboratory setting that is otherwise impossible with live GNSS signals. Spirent GSS7000 simulator takes vehicle motion or vehicle reference coordinates as input, simulates GNSS signals to be received by a GNSS receiver. The simulator can generate atmospheric delay in measurements and can incorporate receiver clock bias if a real receiver is not available in the simulation. The Spirent GSS7000 simulator provides several observable types of different systems. Satellite constellation, atmospheric model, antenna pattern, scenario can be easily specified to meet demands of research and development. In addition, a real receiver makes it possible to simulate multipath and more realistic signals via an external receiver port.

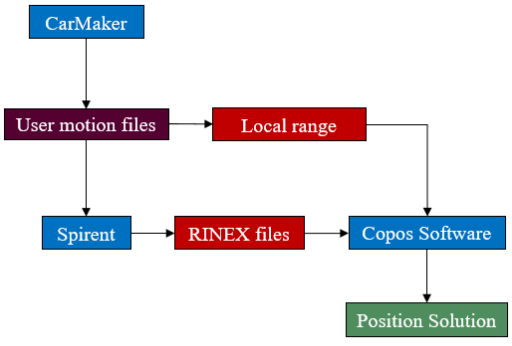

Figure 3: Simplified overview of the simulation framework

The whole simulation procedure is shown in Figure 3. CarMaker is used to generate the user motion files, which are used as input to the Spirent simulator to get RINEX files (observation and navigation). For each simulation epoch, one extracts GNSS measurements from RINEX observation files, computes the satellites' position and velocity and calculates local ranges from vehicles' reference position in user motion files. Finally, the EKF is used to compute the position of each vehicle as described above.

- Ray Tracing Software

The raytracing is performed according to geometrical considerations. Since the true position of every vehicle as well as position of every satellite are known precisely in the simulation environment, the line of sight rays can be determined. The echoes (the reflected rays) are subsequently determined by the mutual geometry of satellites, reflectors and receivers. The reflecting buildings are modelled as concrete, with the corresponding permittivity and conductivity. After the reflected rays are determined, the corresponding signal parameters, namely path delay, the reflection loss and Doppler offset are calculated for each reflected ray. The signals with the calculated parameters are simulated by Spirent and processed by a GNSS receiver.

Figure 4 below gives an example of ray tracing for three cars in an urban environment.

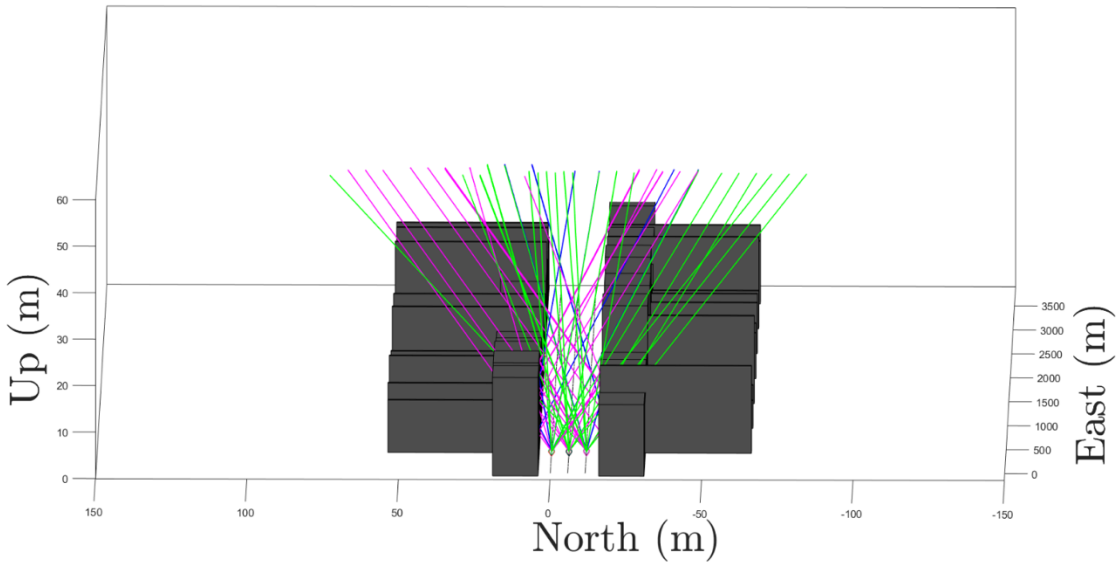

Figure 4: Ray tracing example, green: LOS signals, magenta: NLOS signals, blue: NLOS+LOS signals

The above method allows ray tracing of complicated reflection surfaces. Figure 5 shows an example of a reflecting surface (a wall) used in the simulation. The height profile of the walls is generated from a Rician distribution with a certain mean height and standard deviation, given values are typically, 12m and 3m, as buildings of approximately 3-4 stories in the city.

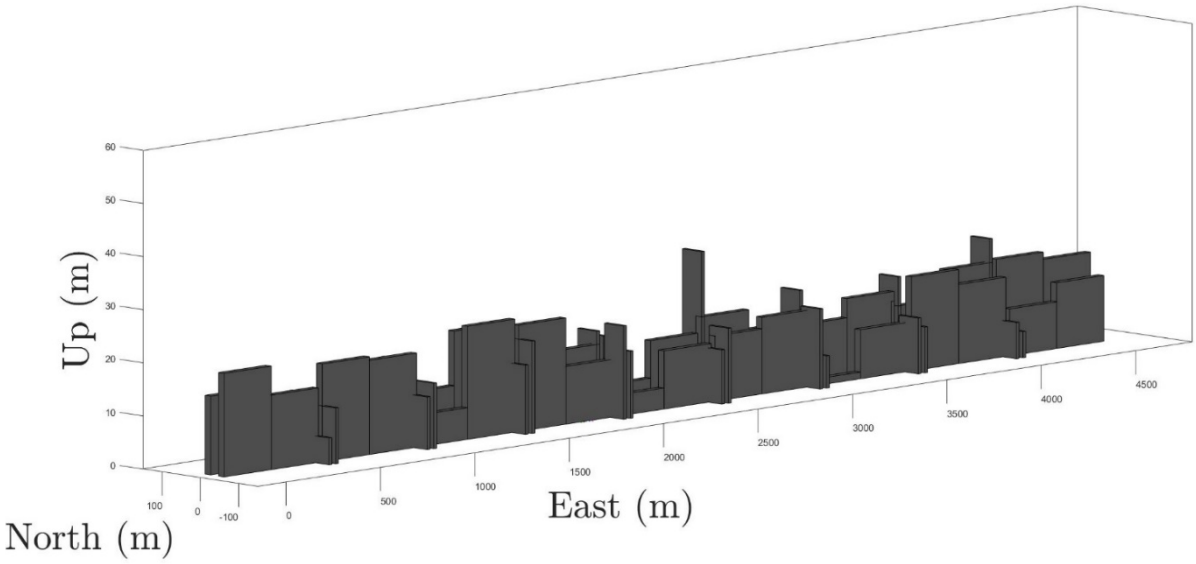

Figure 5: Example of a wall used in ray tracing

It should be noted that the environment simulated corresponds to harsh environment with severe multipath and low share of line of sight GNSS signals. Table 1 below provides an overview of the statistics of signal types in both scenarios.

Table 1
Signal characteristics in the simulated scenarios (ego vehicle)

	Multipath	LOS	NLOS	Blocked
Line	10.0%	56.2%	15.4%	18.4%
Square	4.2%	42.7%	25.7%	27.4%

5. Performance Analysis

In this section, the influence of user geometry and number of users are given to analyze the positioning results of CoPos and SPP of one ego vehicle. The positioning results of SPP are given by EKF using pseudorange measurements of the ego vehicle.

- Influence of user geometry

A scenario with five vehicles moving in a straight line with a constant velocity of 30km/h is simulated in CarMaker. Two vehicles follow the ego vehicle and the other two vehicles move in parallel with the ego vehicle in an open-sky environment (see Figure 6). The local ranges between every vehicle to its neighbors are about 30 meters. The duration of the simulation is 120 seconds. As shown in Figure 6, different vehicle combinations are selected to do CoPos and the positioning accuracy of the ego vehicle in North-South and East-West directions is analyzed by comparing the positioning results obtained by SPP and CoPos with its reference position obtained by CarMaker. The GDOP of SPP and CGDOP of CoPos are compared with each other as well.

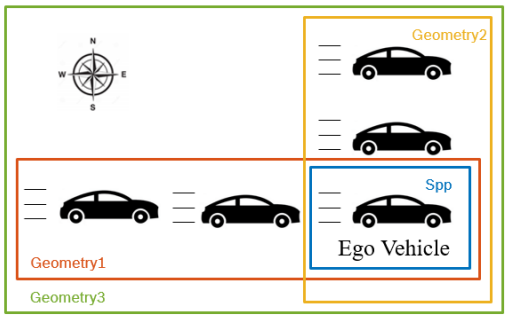

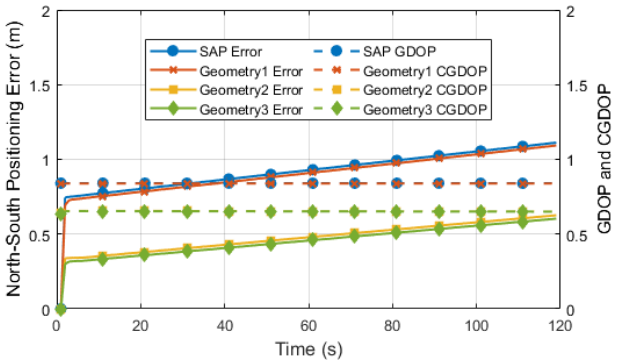

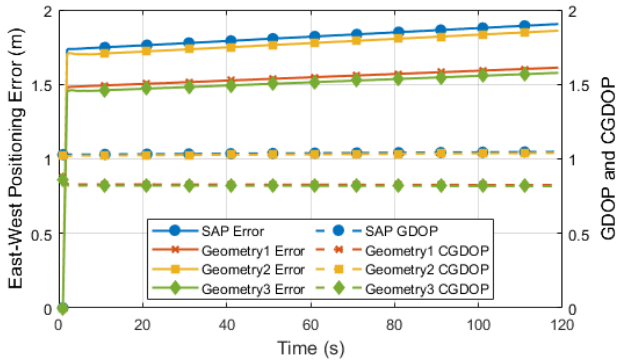

Figure 6: A simple scenario with five moving vehicles, positioning results of SPP and CoPos, GDOP and CGDOP of the ego vehicle

One can see clearly from this scenario that after the initial convergence of the solution caused by EKF, the accuracy of CoPos is superior to the SPP in both East-West and North-South directions. The increasing position error over time is because of the changing of satellite geometry. Different geometries of vehicle group have different performances. In geometry 1, two vehicles are located in the west direction of the ego vehicle, the positioning result has a significant improvement in East-West direction, however, in North-South direction which keeps almost unchanged. The local range measurements in East-West direction are additional measurements for the ego vehicle other than the satellite measurements, which can decrease the CGDOP in that direction. The lower value of CGDOP means the better confidence in positioning solution, as a result, the positioning accuracy can be improved in the direction of the local range component. The geometry 2 contains three vehicles and two of them are in the north of the ego vehicle. The performance of CoPos is opposite to geometry 1. The local range measurements are in the North-South direction therefore the improvement of positioning accuracy is mainly in the North-South direction and the performance of CGDOP provides a consistent result. All the five vehicles in geometry 3 participate in CoPos and the positioning accuracy of the ego vehicle is improved by about 0.5 meter in both East-West and North-South directions. The CGDOP of geometry 3 also has a minimum value in two directions. The results indicate that the CoPos performance is influenced by user geometry and the positioning accuracy will increase corresponding to the direction of local range measurement.

- Influence of the number of users

By using CarMaker, a scenario with fifteen vehicles moving around a rectangle is built. The length and width of this rectangle are 80 meters and 70 meters, respectively. Vehicles are distributed one by one in an open-sky environment. The average velocity of each vehicle is about 20km/h, it will slow down when turning and speed up after entering the straight road. The duration of the whole simulation is 120 seconds. In this scenario, different numbers of vehicles are selected to do CoPos and the positioning results of the ego vehicle that is marked by a green circle are presented in Figure 7.

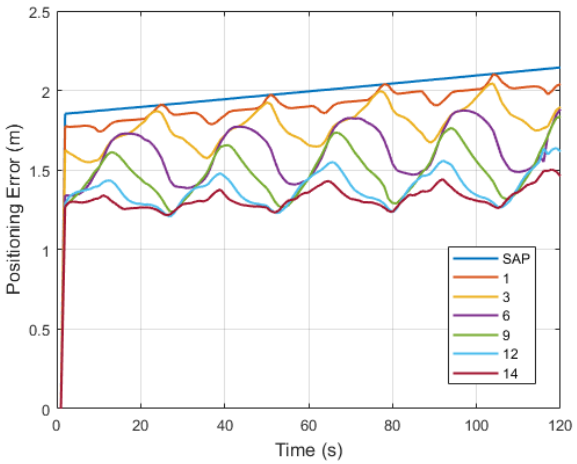

Figure 7: A scenario with fifteen vehicles moving around a square, positioning results of SPP and CoPos with different number of vehicles

It is obvious that SPP error, the dark blue curve, is larger than CoPos ones. The positioning results of CoPos have a wavy performance, the maximum value of each curve occurs when the local ranges are basically in the same direction. Since the geometry of vehicle group changes with time, the positioning results have the corresponding trend. The wavy performance becomes weaker as the number of vehicles increases which means the local ranges are in almost all directions. The small ups and downs of the curves are because of the changing of velocity when vehicles enter the crossroads. With measurements from other fourteen vehicles, the positioning error of the ego vehicle is greatly decreased to about 1.3 meters, compared with SPP accuracy 2 meters. It indicates the accuracy of CoPos increases with the growing number of measurements.

- Multipath mitigation

As shown above, user geometry influences the positioning of users in CoPos. Figure 8 shows three different constellations of five cars used for simulation of multipath scenarios.

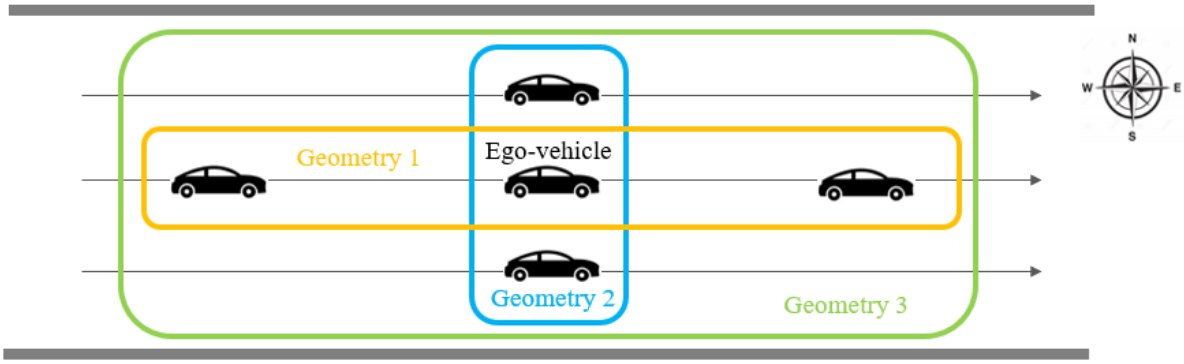

Figure 8: Three different geometries used for simulation of five moving cars in multipath scenarios

In the Figures 9 - 14 below the results of simulation of different user geometries for two scenarios are given. The first scenario is movement in a square in urban canyon, the second one is movement in a straight line with two walls parallel to the street. It is clear from the Figures 9 - 14 that CoPos provides better positioning results than SPP, however, only a combination of multipath mitigation algorithm with CoPos provides positioning significantly better than SPP. The following abbreviations are used in Figures 9 - 14: CP for CoPos, ND for NLOS detection.

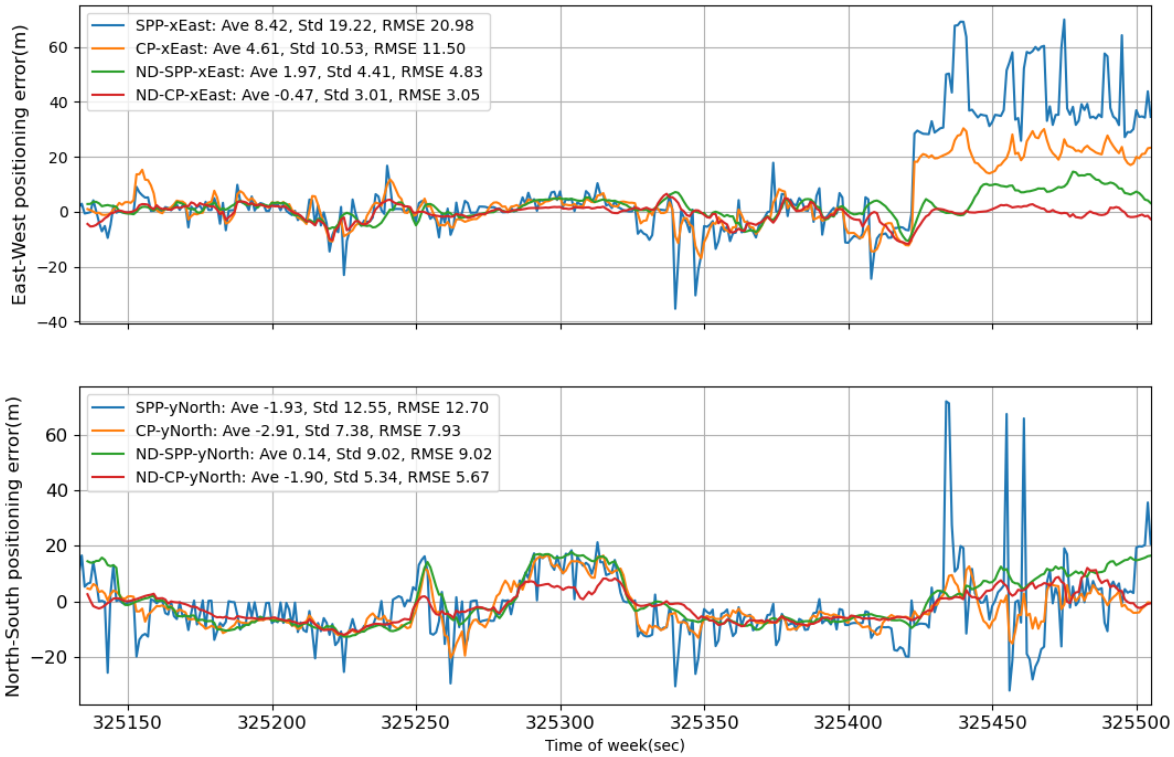

Figure 9: Moving in a square. Positioning accuracy for different positioning types.

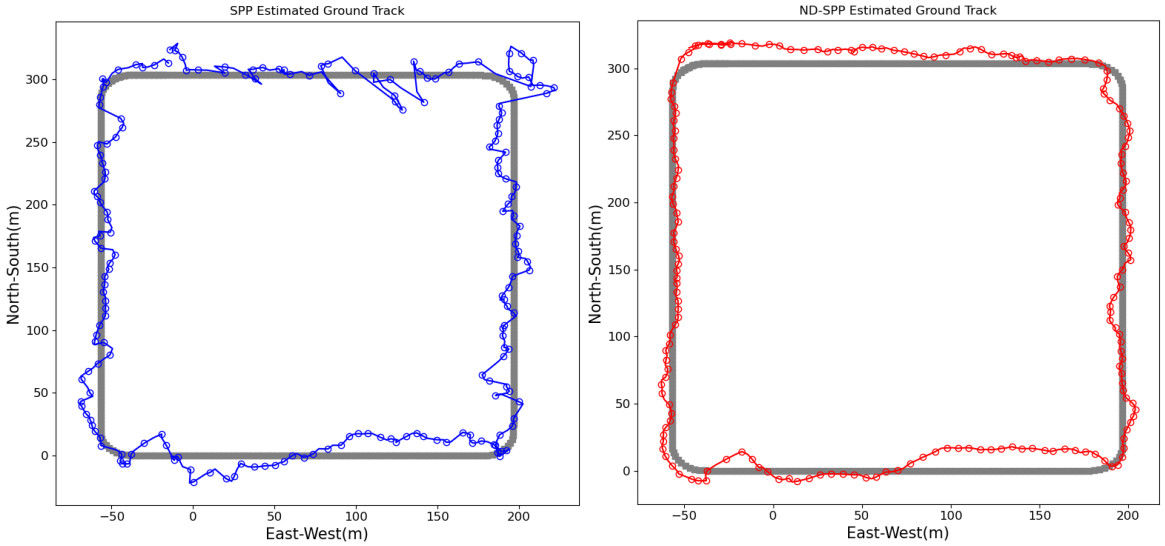

(a) SPP (b) ND-SPP

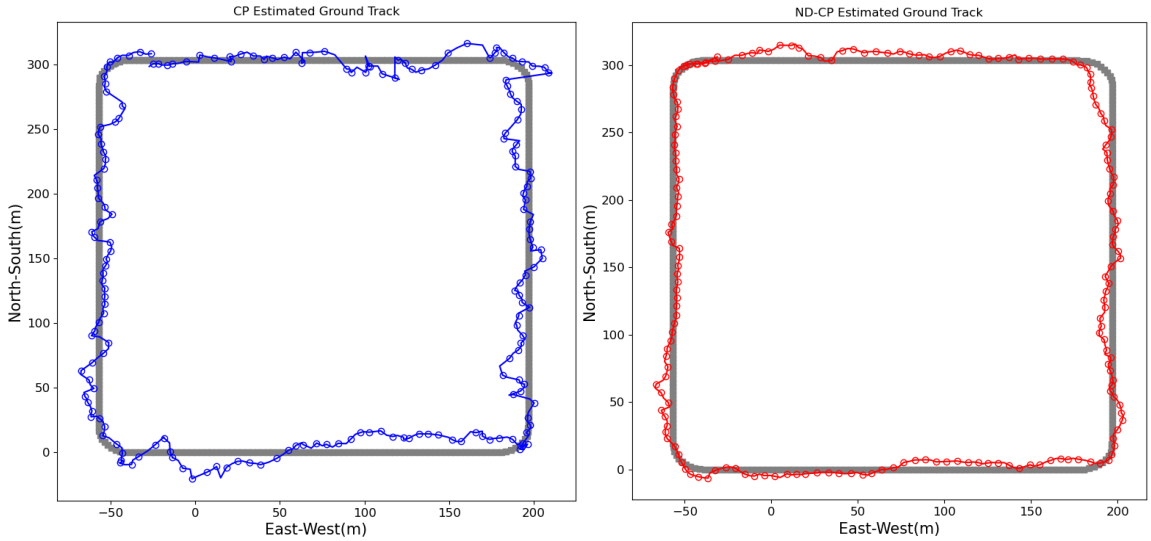

(c) CP (d) ND-CP

Figure 10: Moving in a square. Ground track for different positioning types

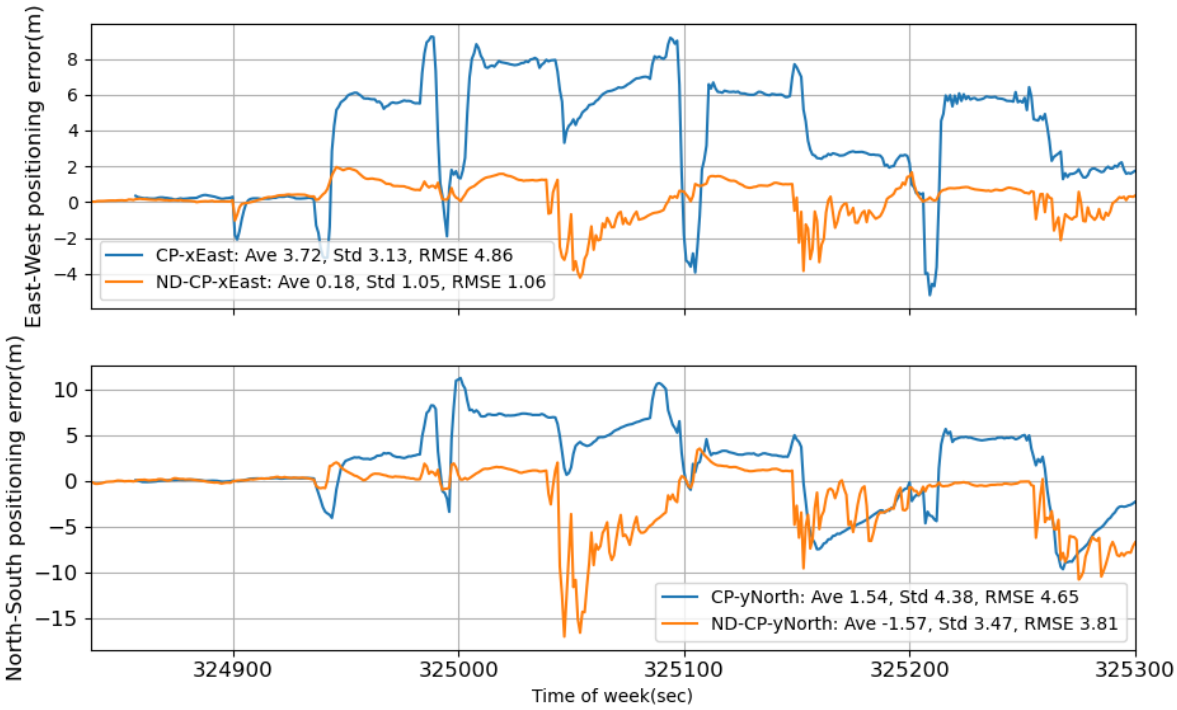

Figure 11: Moving in a straight line. Positioning accuracy for Geometry 1

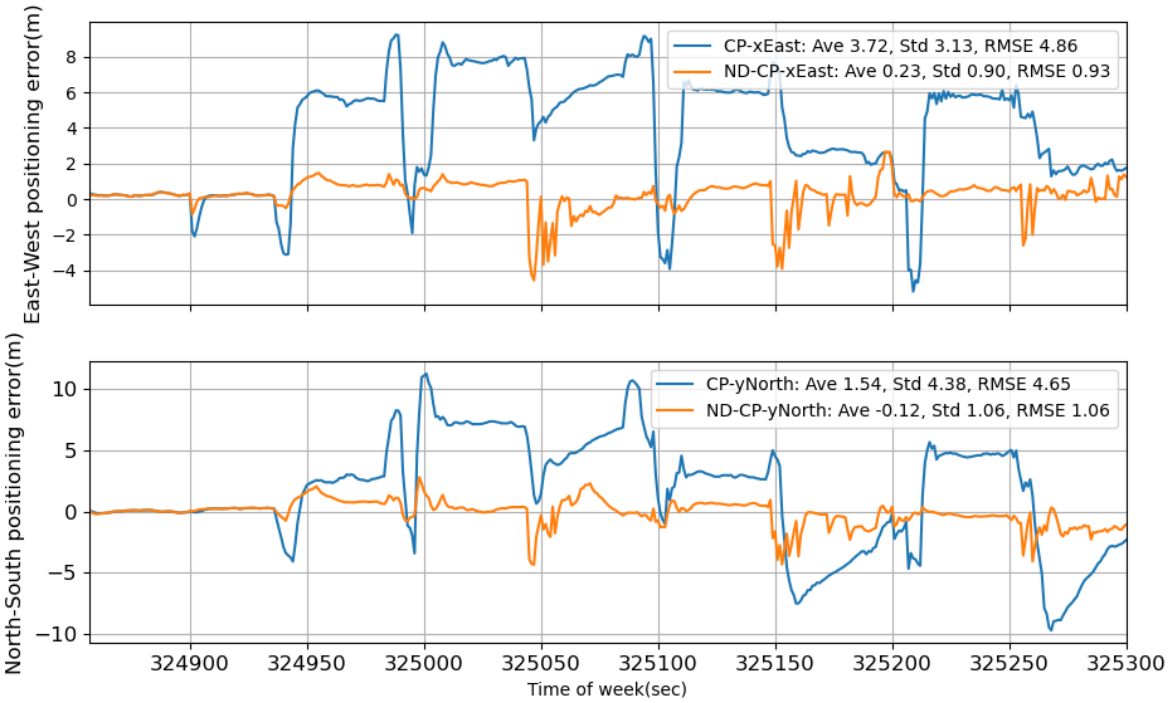

Figure 12: Moving in a straight line. Positioning accuracy for Geometry 2

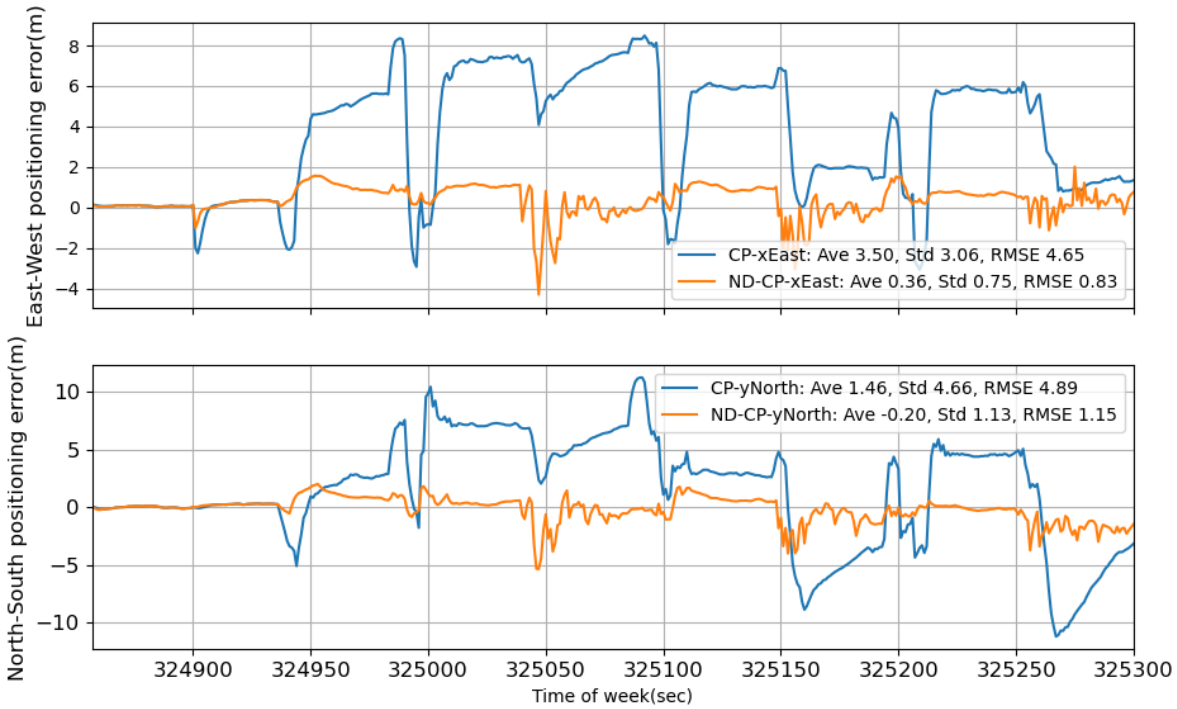

Figure 13: Moving in a straight line. Positioning accuracy for Geometry 3

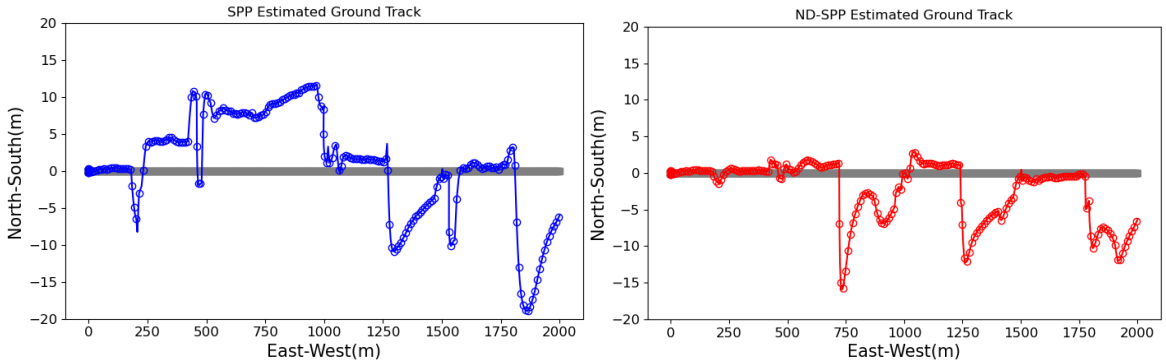

(a) SPP

(b) ND-SPP

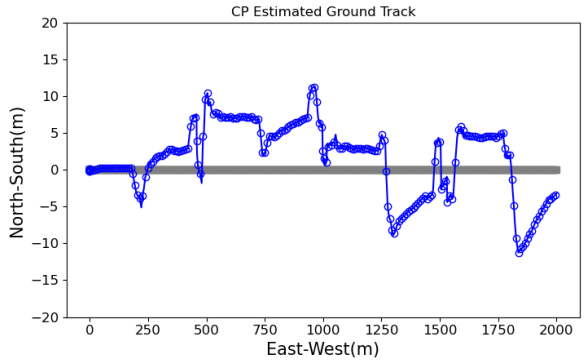

(c) CP

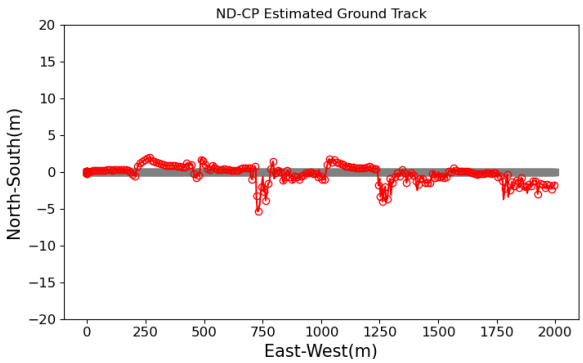

(d) ND-CP

Figure 14: Moving in a straight line. Ground track for different positioning types

6. Conclusions

In this paper, observation models of pseudorange and local range and a collaborative positioning method are presented. A simulation framework based on CarMaker and Spirent is developed. The performance of CoPos is analyzed by using the defined CDOP and the positioning results. The simulation in two scenarios verifies that the positioning accuracy of CoPos is better than SPP and two factors affect its performance: the user geometry and the number of users. The user geometry in different directions will improve the positioning accuracy in the corresponding directions and more dispersed users taking part in CoPos can improve the positioning accuracy significantly.

The multipath mitigation in CoPos is considered too. It is shown with simulations that combination of CoPos and multipath mitigation improves the positioning results significantly even for the scenarios of harsh urban canyon environment.

However, the effect of more vehicles making use of the V2X channel may lead to trade-off, as messages are more likely to be dropped. This problem along with realistic communication channel simulation is subject to future work.

7. Acknowledgements

Authors would like to express their great appreciation to professor Urs Hugentobler (Technical University of Munich) for his patience, enthusiastic encouragement and useful critiques of this research work.

8. References

[1] G. Seco-Granados, J. Lopez-Salcedo, D. Jimenez-Banos and G. Lopez-Risueno. "Challenges in indoor global navigation satellite systems: Unveiling its core features in signal processing." IEEE Signal Processing Magazine 29.2 (2012): 108-131.

[2] N. Patwari, A.O. Hero, M. Perkins, N. S. Correal, and R. J. O'dea. "Relative location estimation in wireless sensor networks." IEEE Transactions on Signal Processing 51.8 (2003): 2137–2148

[3] N. Patwari, J.N. Ash, K. Spyros, A.O. Hero, L. Randolph, Moses, and N.S. Correal. "Locating the nodes: Cooperative localization in wireless sensor networks." IEEE Signal Processing Magazine 22.4 (2005): 54–69.

[4] A. I. Mourikis and S. I. Roumeliotis. "Performance analysis of multirobot cooperative localization." IEEE Transactions on Robotics 22.4 (2006): 666–681.

[5] F. de Ponte Müller. "Survey on ranging sensors and cooperative techniques for relative positioning of vehicles." Sensors 17.2 (2017): 271.

[6] ETSI TR 103 562. "Intelligent Transport Systems (ITS); Vehicular Communications; Basic Set of Applications; Analysis of the Collective Perception Service (CPS); Informative Report for the Collective Perception Service." European Telecommunications Standards Institute (ETSI), 2019

[7] P.D. Groves and Z. Jiang. "Height aiding, C/N 0 weighting and consistency checking for GNSS NLOS and multipath mitigation in urban areas." The Journal of Navigation 66.5 (2013): 653-669.

[8] B. Huang, Z. Yao, X. Cui, M. Lu and J. Guo. "GNSS collaborative positioning and performance analysis." 2014 27th International Technical Meeting of The Satellite Division of the Institute of Navigation (ION GNSS+ 2014), Florida, USA, 2014.

[9] B. Huang, Z. Yao, X. Cui, and M. Lu. "Dilution of precision analysis for GNSS collaborative positioning." IEEE Transactions Vehicular Technology 65.5 (2015): 3401-3415.

[10] H. Ko, B. Kim, and S.H. Kong. "GNSS multipath-resistant cooperative navigation in urban vehicular networks." IEEE Transactions Vehicular Technology 64.12 (2015): 5450-5463.

[11] F. A. Schiegg, S. Li, and N. Mikhaylov. "TEPLITS: A comprehensive Test Platform for Intelligent Transportation Systems." 2020 IEEE 90th Vehicular Technology Conference (VTC2020-Spring), Antwerp, Belgium, 2020.

[12] F. A. Schiegg, J. Krost, S. Jesenski and J. Frye. "A Novel Simulation Framework for the Design and Testing of Advanced Driver Assistance Systems." 2019 IEEE 90th Vehicular Technology Conference (VTC2019-Fall), Honolulu, HI, USA, 2019.

[13] R. Brown and P. Hwang, Introduction to random signals and applied Kalman filtering, Wiley, New York, NY, 1992.

[14] F. K. Brunner, H. Hartinger, and L. Troyer. "GPS signal diffraction modelling: the stochastic SIGMA-Δ model." Journal of Geodesy 73.5 (1999): 259-267.

[15] J. J. Spiker, The Global Positioning System: Theory and Application, American Institute of Aeronautics and Astronautics: Washington, DC, USA, 1996.

[16] A. Papoulis, Probability, Random Variables, and Stochastic Processes, 3rd ed., McGraw-Hill, New York, NY, 1991.